

Thermocapillary migration of droplets under molecular and gravitational forces

J. R. Mac Intyre^{1,†}, J. M. Gomba¹, Carlos Alberto Perazzo^{2,3}, P. G. Correa¹
and M. Sellier⁴

¹Instituto de Física Arroyo Seco - IFAS (UNCPBA) and CIFICEN (UNCPBA-CICPBA-CONICET),
Pinto 399, 7000, Tandil, Argentina

²IMeTTyB, Universidad Favaloro-CONICET, Solís 453, C1078AAI Buenos Aires, Argentina

³Departamento de Física y Química, FICEN, Universidad Favaloro, Sarmiento 1853,
C1044AAA Buenos Aires, Argentina

⁴Department of Mechanical Engineering, University of Canterbury, Private Bag 4800,
Christchurch 8140, New Zealand

(Received 3 July 2017; revised 11 January 2018; accepted 7 April 2018;
first published online 17 May 2018)

We study the thermocapillary migration of two-dimensional droplets of partially wetting liquids on a non-uniformly heated surface. The effect of a non-zero contact angle is imposed through a disjoining–conjoining pressure term. The numerical results for two different molecular interactions are compared: on the one hand, London–van der Waals and ionic–electrostatics molecular interactions that account for polar liquids; on the other hand, long- and short-range molecular forces that model molecular interactions of non-polar fluids. In addition, the effect of gravity on the velocity of the drop is analysed. We find that for small contact angles, the long-time dynamics is independent of the molecular potential, and the footprint of the droplet increases with the square root of time. For intermediate contact angles we observe that polar droplets are more likely to break up into smaller volumes than non-polar ones. A linear stability analysis allows us to predict the number of droplets after breakup occurs. In this regime, the effect of gravity is stabilizing: it reduces the growth rates of the unstable modes and increases the shortest unstable wavelength. When breakup is not observed, the droplet moves steadily with a profile that consists in a capillary ridge followed by a film of constant thickness, for which we find power law dependencies with the cross-sectional area of the droplet, the contact angle and the temperature gradients. For large contact angles, non-polar liquids move faster than polar ones, and the velocity is proportional to the Marangoni stress. We find power law dependencies for the velocity for the different regimes of flow. The numerical results allow us to shed light on experimental facts such as the origin of the elongation of droplets and the existence of saturation velocity.

Key words: drops, lubrication theory, thermocapillarity

† Email address for correspondence: jmintyre@exa.unicen.edu.ar

1. Introduction

The migration of droplets over a solid substrate is a long-standing topic of interest in academia and crucial in several situations of practical importance (Oron, Davis & Bankoff 1997; Craster & Matar 2009). This scenario is commonly encountered in a variety of industrial applications, such as coating, ink-jet printing, microfluidics and micro-electronics, and medical diagnostics (Huebner *et al.* 2008; Casadevall i Solvas & DeMello 2011; Choi *et al.* 2012; Campana *et al.* 2016). These technological processes make use of different physical principles to displace the liquids, which includes electro-osmotic forces, electrohydrodynamic, thermocapillarity, chemical gradients, centrifugation and magneto-hydrodynamics (Cachile *et al.* 2002; Stone, Stroock & Ajdari 2004; Ubal *et al.* 2008). In particular, the thermocapillary effect, which concentrates our attention here, has been employed in a large number of microfluidic devices to actuate droplets and bubbles given that the change of the surface tension with temperature is observable in most liquids (Karbalaeei, Kumar & Cho 2016).

Among the wide variety of possible configurations proposed in the literature for the displacement of droplets, we focus on droplets on horizontal surfaces that are driven by thermocapillary forces. A sessile drop over a non-uniformly heated substrate undergoes a shear stress along the surface of the liquid that moves the droplet from warmer to colder regions. The motion is quite complex and disagreement in the current knowledge of the topic clearly indicates the need for more detailed understanding of the dynamics of these flows (Karbalaeei *et al.* 2016).

There is a large volume of published studies describing the thermocapillary motion of droplets. Brochard-Wyart (1989) analysed the motion of a wedge-shape drop in the presence of both chemical and thermal gradients. The droplet may move to hot or cold regions depending on the selected liquid–substrate system. The result is analogous to the Soret effect in binary mixtures, where it is well known that a solute can move toward either the cold or the hot region. Ford & Nadim (1994) extended the study to a steady drop with an arbitrary but fixed shape, and derived a general analytical expression for the velocity using the Navier slip condition. They assumed different contact angles at the rear and leading fronts, and found a threshold depinning force that depends on the applied temperature gradient. Smith (1995) also assumed slipping at the liquid solid interface, but introduced a dynamic boundary condition that relates the contact line speed with the contact angle. He treated the steady state case and found two possible regimes: either a droplet moving with a constant velocity and fixed profile or a pinned (cylindrical) droplet with an inner circulation flow.

Gomba & Homay (2010) studied the problem using a precursor film model at the contact line. One crucial difference with previous works is that they solve an initial value problem for the displacement of the droplet, without imposing restrictions on neither the shape of the interface nor the velocity of the contact lines. This approach allowed the authors to find other solutions different from the steady ones reported before. They carried out a parametric study using the contact angle and they distinguished three different flow regimes. For small contact angles, the drop spreads in the direction of motion, while for large contact angles the liquid migrates steadily preserving its shape. For intermediate contact angles, the authors alluded to a transient complex dynamics where the droplet breaks up into smaller droplets but did not investigate this regime exhaustively. One of our goals here is to shed light on this rich flow regime.

More recently, Karapetsas, Sahu & Matar (2013) also solved an initial value problem and analysed the spreading of droplets initially far from equilibrium and

cases where the surface energies depend on the temperature. They showed that for constant equilibrium contact angles, the substrate temperature gradients combined with gravity give rise to enhanced spreading rates, characterized by exponents as large as $2/3$, larger than those predicted by Tanner's law. For cases where the surface energy changes with temperature, they observed a rather complex dynamics that includes the non-monotonic displacements of drops and stick–slip movements of the contact line. Chaudhury & Chakraborty (2015) compared 'normal' and 'self-rewetting' fluids. In the first the surface tension presents a linear dependence with temperature, while in the second the relationship is quadratic. They found power laws for the width of small-contact-angle droplets with time, that are in good agreement with the results of Gomba & Homay (2010) and Karapetsas *et al.* (2014), respectively. Diametrically opposed, Nguyen & Chen (2010) focused on large-contact-angle droplets and found that non-wetting liquids (i.e. contact angles larger than 90°) are faster than those with contact angles just below 90° . They explained this difference in terms of the large internal convection observed for the smaller angle case, that opposes to the Marangoni stress.

The theoretical models and their predictions are partially validated by the available experimental literature. Brzoska, Brochard-Wyart & Rondelez (1993) and Chen *et al.* (2005) found a threshold in the temperature gradient at which the droplet migrates with a fixed shape or, below the threshold, the drop may not move due to the contact-angle hysteresis. Brzoska *et al.* (1993) also concluded that above this critical value, the velocity of the droplet is proportional to the temperature gradient and inversely proportional to the viscosity, in agreement with Brochard-Wyart (1989) and Gomba & Homay (2010). Additionally, Chen *et al.* (2005) compared the experimental results with the predictions of a theoretical expression derived by Ford & Nadim (1994) and found that the fitting of the experimental values is more sensitive to contact angle hysteresis than to the magnitude of the slip length. Pratap, Moumen & Subramanian (2008) reported experiments of decane droplets on a polydimethylsiloxane (PDMS)-coated surface. In this case, the significant distortion observed in the footprint of the drop from a circular shape is compatible with the modelling of Karapetsas *et al.* (2013), where the surface energies (and contact angles) vary with the local temperature. The evolution into a film predicted by Gomba & Homay (2010) for vanishingly small contact angles resembles the profiles obtained in the experiments of Sur, Bertozzi & Behringer (2003), while the dependence of the velocity on the thermal gradient and viscosity, for droplets that move keeping their shape, are compatible with experiments reported by Chen *et al.* (2005). Interestingly, Dai *et al.* (2017) showed experiments where a thin film fluid is deposited behind the droplet, as observed in the simulations of Gomba & Homay (2010).

Other theoretical predictions seem to lack correlated experimental support. For instance, the occurrence of the breakups for intermediate contact angles, which is one of main goals of this article. In the experiments of Brzoska *et al.* (1993), where the authors employ PDMS on hydrophobic surfaces and the contact angle is $\theta = 13^\circ$, the larger volumes should break up into smaller droplets according to Gomba & Homay (2010). Nevertheless, the experiments show that the droplets enlarge and displace as a single droplet. Another open issue is the relationship between the displacement velocity U and the footprint R . The model of Brzoska predicts a linear dependence for small droplets that it is not observed in Chen *et al.* (2005) experiments for alkane hydrocarbons, despite the volumes are comparable with the smallest ones of Brzoska *et al.* (1993). On the other hand, the modelling of Gomba & Homay (2010), under non-gravity conditions, predicts that $U \propto A(R)^{0.4}$, A being the cross-sectional area of the droplet.

In particular, Brzoska *et al.* (1993), who performed experiments for a wider range of volumes than Chen *et al.* (2005), presented results that triggered some of the questions that motivated the present work. For example, the experiments show a change in the curve U versus R , from a linear law for the smallest droplets to a weaker dependence with R for larger volumes, suggesting a saturation for $R \rightarrow \infty$. Also, larger droplets present an elongation in the direction of displacement. Brzoska and collaborators attribute the saturation in U and the elongation of droplets to the effect of gravity. The elongation of droplets in their experiments is also observed in the simulations by Gomba & Homsy (2010). Nevertheless, the theoretical results predict that the elongation in the experiments of Brzoska *et al.* (1993) with the largest areas and the strongest thermal gradients ($\nabla T = 1 \text{ C mm}^{-1}$) must be followed by a breakup into smaller droplets. The breakup has not been reported in experiments.

After review of the available experimental data, we observe that all the experiments were performed with non-polar liquids (polydimethylsiloxane and alkane hydrocarbons), while the modelling employed by Gomba & Homsy (2010) is adequate for polar liquids (Starov, Velarde & Radke 2007; Mac Intyre, Gomba & Perazzo 2016). The disagreement between theory and experiments, and also the differences in the experimental results, suggest that the dynamics may depend on the polarity of the liquid. Furthermore, the experiments were made under gravity conditions and thus, it should be included in the modelling to evaluate its role in the saturation of U and the elongation of the droplets.

Summarizing, our ultimate goal here is to understand the origin of the mentioned disagreements by exploring the effects of the polarity of liquids and the gravity on the velocity of the travelling droplets and the occurrence of breakups. In the present work different flow regimes are identified, the drop velocity for each regime is determined, and the non-occurrence of breakup in the large volume experiments is explained. In addition, simulations with gravity included are presented in order to ascertain its effect on morphology, velocity and stability of the drop.

The article is organized as follows. In §2, we present the mathematical modelling for the droplet evolution. In §3, we describe the flow of droplets with small contact angles and demonstrate the independence of the dynamics from the molecular potential. In §4, we present the behaviour of the droplets for intermediate contact angles. We show that, depending on the polar nature of the liquid, the droplets migrate with a steady profile or break up into a smaller droplets. A study of the stability of the thickness profile sheds light on whether or not breakup is observed. In §5, we focus on the large-contact-angle regime of flow. There, we show that droplets migrate keeping their initial shape for both potentials and when we include the gravity, the shape of the droplets modifies only slightly from their initially steady shape. Finally, in §6 we present the discussions and conclusions.

2. Mathematical model

We consider a two-dimensional droplet of density ρ and viscosity μ deposited on a non-uniformly heated surface, as shown in figure 1. Under the assumptions of lubrication approximation, the Navier–Stokes equations are reduced to a single partial differential equation for the thickness h of the droplet. Although this approximation assumes small slope of the liquid–gas interface, it is usually employed to describe partial wetting systems. Its applicability was studied and small differences of a few per cent were found when compared with solutions of the Navier–Stokes equation for contact angles as large as 40° (Goodwin & Homsy 1991; Perazzo & Gratton 2004).

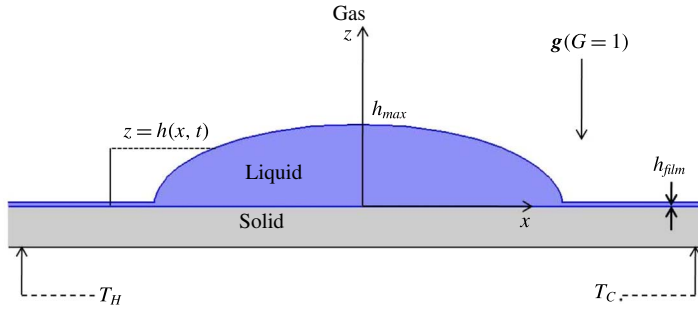


FIGURE 1. (Colour online) Sketch of the problem: a two-dimensional droplet of thickness $h(x, t)$ resting on a non-uniformly heated surface. The temperature induces a gradient of the surface tension which drives the liquid towards the region with the highest surface energy. The droplet is surrounded by a constant film thickness with an initial (equilibrium) thickness h_{film} (Mac Intyre *et al.* 2016).

The flow field $u(x, z, t)$ is governed by the momentum balance equation (Oron *et al.* 1997; Craster & Matar 2009)

$$\mu \frac{\partial^2 u}{\partial z^2} - \frac{\partial p}{\partial x} = 0, \tag{2.1}$$

and the flow continuity

$$\frac{\partial h}{\partial t} + \frac{\partial}{\partial x} \left(\int_0^h u \, dz \right) = 0, \tag{2.2}$$

where $h = h(x, t)$ is the thickness profile of the drop. The second term in (2.1) is given by

$$\frac{\partial p}{\partial x} = \frac{\partial}{\partial x} \left(-\gamma \frac{\partial^2 h}{\partial x^2} - \Pi(h) + \rho gh \right), \tag{2.3}$$

γ being the surface tension and g the gravity. The term $\Pi(h)$ represents the disjoining–conjoining pressure defined by (Oron *et al.* 1997; Schwartz & Roy 2004)

$$\Pi(h) = \kappa \left[\left(\frac{h_*}{h} \right)^n - \left(\frac{h_*}{h} \right)^m \right], \quad n > m > 1. \tag{2.4}$$

The thickness of the energetically favoured molecular film is represented by h_* and κ is related to the static contact angle θ by (Schwartz & Eley 1998)

$$\kappa = \frac{\gamma \tan^2 \theta (n - 1)(m - 1)}{2(n - m) h_*}. \tag{2.5}$$

The contact angle θ is defined as the angle at the inflection point for large drops (Schwartz & Eley 1998; Gomba & Homsy 2009). Once θ is chosen, the value of κ is determined and, therefore θ quantifies the strength of the molecular interaction between the liquid and the substrate (the relationship among κ , the Hamaker

constants and θ is discussed in Solomentsev & White (1999) and Mac Intyre *et al.* (2016)).

The definition in (2.4) has been largely employed to model the effects of molecular interactions. Here, we focus on two different types of molecular potential. On the one hand, the case $(n, m) = (3, 2)$ that represents the competition of London–van der Waals ($n = 3$) and ionic–electrostatics forces ($m = 2$) (Schwartz & Eley 1998; Gotkis *et al.* 2006). The dependence with $m = 2$, valid for thickness much lower than the Debye length, was verified in experiments of water (polar liquid) films on glass, quartz and mica (Derjaguin & Churaev 1974). The term with $m = 3$ is an exact classical result obtained by summing individual London–van der Waals interactions between molecules. On the other hand, the case $(n, m) = (4, 3)$ that correctly describes retarded and non-retarded effects in London–van der Waals interactions, as in experiments with tetradecane on quartz and hexane on metals (Derjaguin & Churaev 1974; Derjaguin, Rabinovich & Churaev 1978; Starov *et al.* 2007). The term with $n = 4$ is an exact expression that results from considering retardation effects in London–van der Waals interactions (Oron & Bankoff 2001; Glasner & Witelski 2003; Starov *et al.* 2007). Summarizing, the pairs $(3, 2)$ and $(4, 3)$ model the molecular interactions for polar and non-polar liquids, respectively.

Equation (2.1) is subject to two boundary conditions: no slip at the solid substrate and tangential Marangoni stress along the liquid–air interface (Ehrhard & Davis 1991); that is

$$u(x, 0, t) = 0, \quad (2.6)$$

$$\mu \frac{\partial u}{\partial z} \Big|_{z=h} = \frac{d\gamma}{dx} = \frac{d\gamma}{dT} \frac{dT}{dx}. \quad (2.7)$$

The surface tension γ is linear in the temperature $T(x, h)$ at the air–liquid interface (Eötvös 1886; Guggenheim 1945)

$$\gamma = \gamma_0 - \sigma(T - T_0), \quad (2.8)$$

where γ_0 is the surface tension at $T = T_0$ and σ a positive constant. Based on experimental data (Brzoska *et al.* 1993; Chen *et al.* 2005), it is reasonable to assume that the conduction is the main heat transfer mechanism within the drop (i.e. Péclet number $Pe = HU/\delta \ll 1$) and the conductivity of the liquid is high (i.e. Biot number $Bi = Hq_\infty/\kappa_t \ll 1$). Here, H is the maximum droplet thickness, U the migration velocity, δ the liquid thermal diffusivity, q_∞ the interfacial heat transfer coefficient and κ_t the liquid thermal conductivity. Consequently, the unknown temperature T is related to the linear temperature profile at the substrate $T_s(x)$ by means of $T(x, h) = T_s(x)$ (Ehrhard & Davis 1991; Gomba & Homsy 2010) and the boundary condition at the drop air interface becomes

$$\mu \frac{\partial u}{\partial z} \Big|_{z=h} = \frac{d\gamma}{dT} \frac{dT_s}{dx} = \sigma \frac{T_H - T_C}{L} = \tau, \quad (2.9)$$

τ being a positive constant and L the distance of application of the two temperature.

We set the scale in both space directions as $h_c = x_c = a$, where $a = \sqrt{\gamma_0/\rho g}$ is the capillary length, and define the characteristic time as $t_c = 3\mu a/\gamma_0$. Equation (2.2) for the thickness $h(x, t)$ becomes

$$\frac{\partial h}{\partial t} + \frac{\partial}{\partial x} \left[h^3 \frac{\partial}{\partial x} \left(\frac{\partial^2 h}{\partial x^2} + K \left[\left(\frac{h_*}{h} \right)^n - \left(\frac{h_*}{h} \right)^m \right] - Gh \right) + Bh^2 \right] = 0, \quad (2.10)$$

where the constants are

$$K = \frac{\tan^2 \theta (n-1)(m-1)}{2(n-m)h_*}, \quad B = \frac{3a\tau}{2\gamma_0}, \quad (2.11a,b)$$

and h_* is in units of a . The term which models the gravity effect is multiplied by the constant $G = x_c^2 \rho g / \gamma_0$, which in the selected scale results in

$$G = \begin{cases} 1 & \text{with gravity} \\ 0 & \text{without gravity.} \end{cases} \quad (2.12)$$

The evolution equation (2.10) includes capillary, gravity, disjoining and Marangoni effects. This fourth-order differential equation is solved using finite element technique in the COMSOL Multiphysics environment, and is subject to periodic boundary conditions at both extreme of the domain for the height of the droplet h and pressure p . A convergence analysis was carried out to check the accuracy of the calculations, and the results were satisfactory compared with those obtained using a finite difference technique (Gomba & Homsy 2010).

The initial condition in the following simulations corresponds to the profile of a static droplet of area A when the temperature gradient is zero. We employ the static profiles reported by Mac Intyre *et al.* (2016) for a molecular potential with $(n, m) = (4, 3)$ and by Gomba & Homsy (2009), Perazzo, Mac Intyre & Gomba (2014) for $(n, m) = (3, 2)$. Those analytic solutions are scaled using molecular constant κ and, in order to change the scale appropriately, we have to set the thermodynamic contact angle θ in the parameter K in (2.11) (Mac Intyre *et al.* 2016). The profile of the droplet is allowed to change dynamically over time and the contact angle θ plays the role of parametric value. Given that the scale in x and z axes is a , θ has the same value in both dimensional and dimensionless variables.

Table 1 summarize the relevant physical parameters, together with the typical values found in experiments. Based on these parameters, we estimate the range for B as $0.002 \leq B \leq 0.05$. A word about the value of the precursor film thickness is appropriate. When the ratio of the maximum height to the precursor film thickness increases, the use of realistic values for h_* in problems with moving contact lines is impractical because it requires cell sizes of the order of h_* , as shown in Gaskell *et al.* (2004). Then, most of the simulations are solved using $h_* \geq 5 \times 10^{-3} a$.

3. Small contact angle: film regime

3.1. Absence of gravity, $G = 0$

The film regime occurs for small contact angles. Therefore, we have that $\tan^2 \theta \sim 0$, which implies that the molecular action is negligible (Chaudhury & Chakraborty 2015). Experimental results for Marangoni films by Fote, Slade & Feuerstein (1977) have shown that non-polar liquids under microgravity develop a linear profile. Similarly, Sur *et al.* (2003) have shown experimentally a linear profile connecting the advancing ridges with the fluid in the container. Gomba & Homsy (2010) have reported a linear profile numerically and demonstrated an analytical expression for this evolution for polar liquids.

Figure 2 shows the numerical solution of (2.10) for a non-polar liquid with $\theta = 4^\circ$ and $G = 0$. After a short transient stage, the front develops a characteristic capillary ridge and the bulk adopts a linear profile which slope decreases in time. Note

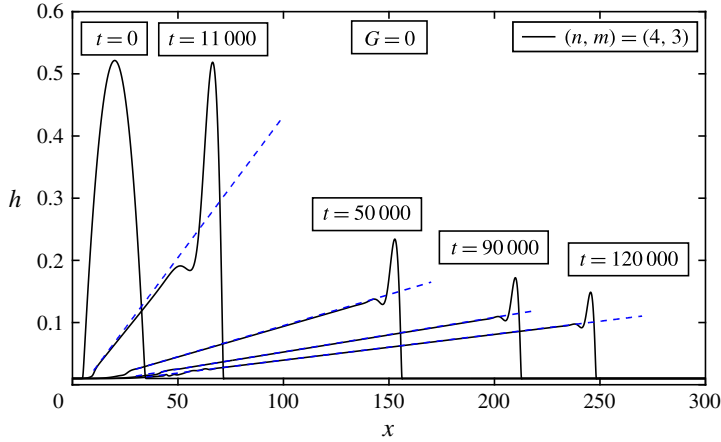


FIGURE 2. (Colour online) Evolution of the thickness profile for a droplet with cross-sectional area $A = 10$, contact angle $\theta = 4^\circ$, thermal gradient $B = 0.01$ and $(n, m) = (4, 3)$. The corresponding profiles for $(n, m) = (3, 2)$ are almost identical to these ones. Here $h_* = 0.01$. The dashed blue line is the analytic solution for the rear profile given by (3.2).

Parameter	Physical quantity	Estimate
μ	Viscosity	10^{-2} Pa s
γ_0	Surface tension	10^{-2} N m $^{-1}$
ρ	Density	10^3 kg m $^{-3}$
$a = \sqrt{\gamma_0/\rho g}$	Capillary length	10^{-4} – 10^{-3} m
dT_s/dx	Thermal gradient	10^2 – 10^3 °C m $^{-1}$
$\sigma = d\gamma/dT $	Variation of γ with T	10^{-5} – 10^{-4} N (m °C) $^{-1}$
h_*	Stable film thickness	10^{-10} – 10^{-9} m
δ	Liquid thermal diffusivity	10^{-8} – 10^{-7} m 2 s $^{-1}$
q_∞	Interfacial heat transfer coefficient	10 W (m 2 °C) $^{-1}$
κ_t	Liquid thermal conductivity	10^{-1} W (m °C) $^{-1}$

TABLE 1. Orders of magnitude of the relevant physical parameters (Brochard-Wyart 1989; Brzoska *et al.* 1993; Schwartz & Eley 1998; Chen *et al.* 2005; Pratap *et al.* 2008).

that the bump forms because the contact line moves slower than the fluid being pumped in from behind by the Marangoni stress. Due to independence of molecular interaction, non-polar liquids exhibits almost identical behaviour to polar liquids. As time increases, the droplet elongates, its maximum height decreases and the volume under the linear profile grows.

The numerical solutions of the differential equation retaining all terms show that the long rear part of the drop develops a linear profile. To describe it analytically, we assume null curvature in this region so that the capillary effect can be neglected and, due to the fact that the molecular forces are negligible, equation (2.10) becomes

$$\frac{\partial h}{\partial t} + \frac{\partial}{\partial x}(Bh^2) = 0. \quad (3.1)$$

Then, the thickness profile is constant along of the characteristic $dx/dt = 2Bh$, which means that a point with height h moves to the right with speed $2Bh$. As a result, the

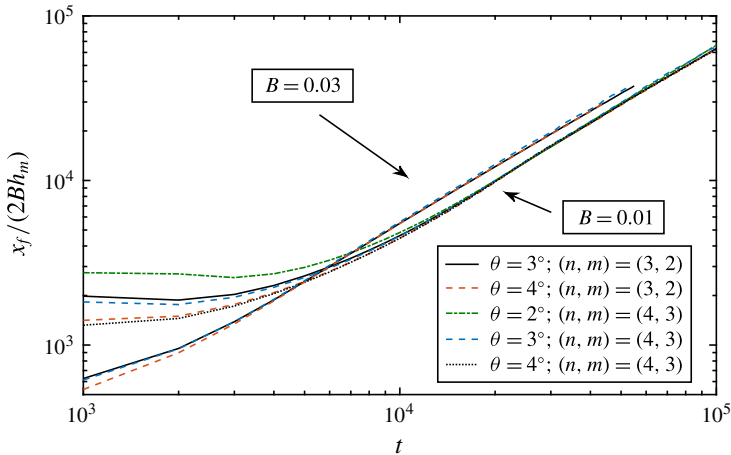


FIGURE 3. (Colour online) Evolution of the front x_f for several values of θ and B with both molecular potentials. Here, $A = 10$, $h_* = 0.01$, $G = 0$ and h_m is the maximum of the profile.

linear profile is (Gomba & Homsy 2010)

$$h = \frac{x - x_0}{2Bt}, \quad (3.2)$$

where x_0 is a constant related to the initial position of the rear contact line. Figure 2 shows the comparison between the numerical solution of the full equation (2.10) with (3.2). The high agreement justifies the omission of surface tension and disjoining pressure terms in (3.1). Figure 3 shows the evolution of the front x_f for several values of θ and B with both polar and non-polar liquids. At long times, the curves converge to the asymptotic curve $x_f/h_m \sim t^{1/2}$ independently of the molecular interaction. Note that as the value of B is increased, the duration of the transient stage is reduced.

The bulk region of the droplet can be approximated by a triangular profile, and then its area A is (Gomba & Homsy 2010)

$$A = \frac{w(x_f - x_a)}{2(2Bt)} = \frac{w^2}{4Bt}, \quad (3.3)$$

with x_a the location of the receding contact line and $w = x_f - x_a$ the droplet width. Then, the width is $w = (4ABt)^{1/2}$ and, therefore, the footprint of the droplet increases with time, as shown in figure 4. In addition, we can see that while the slope of the linear profile is independent of A , as predicted by (3.2), the velocity of the front increases with A and the position x_a is almost constant.

3.2. Effect of gravity, $G = 1$

Figure 5 shows the evolution of the thickness profile under the same conditions as in figure 2 but with $G = 1$. The initial profile, compressed in the z direction due to gravity, evolves to the asymptotic linear profile (3.2). Nevertheless, gravity has a role at the leading front: comparing with the evolution shown in figure 2, we can see that the presence of gravity decreases the height of the capillary ridge and smooths the valley immediately behind it.

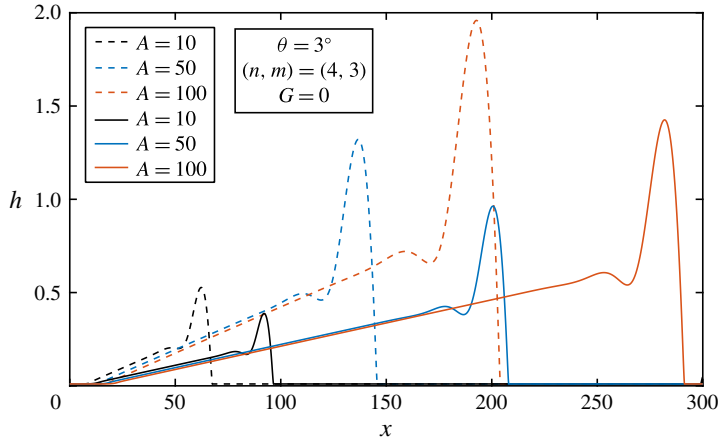


FIGURE 4. (Colour online) Evolution of the thickness profile for several values of A at two different times: $t = 9000$ (dashed lines) and $t = 19000$ (solid lines). The contact angle is $\theta = 3^\circ$, $B = 0.01$, $h_* = 0.01$, $G = 0$ and $(n, m) = (4, 3)$. The linear profile is given by (3.2).

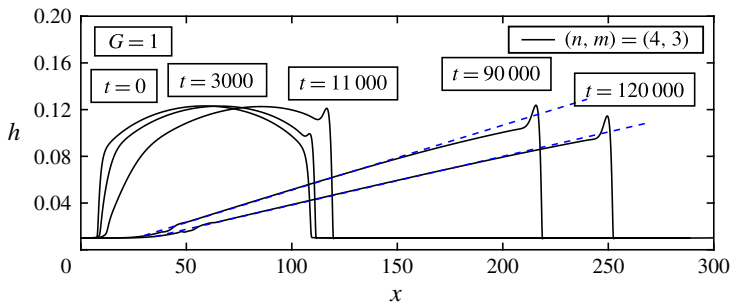


FIGURE 5. (Colour online) Evolution of the thickness profile for a droplet with $A = 10$, $\theta = 4^\circ$, $B = 0.01$, $G = 1$, $(n, m) = (4, 3)$ and $h_* = 0.01$. The dashed blue line is the analytic solution (3.2). Similar behaviour is observed for a molecular potential with $(n, m) = (3, 2)$.

The most remarkable effect of gravity is on the velocity of the front, as shown in figure 6. Given that the initial profiles for $G = 1$ and $G = 0$ have the same initial front position, in figure 6(a) we observe that the profile with $G = 1$ takes more time to reach the asymptotic linear shape than the case $G = 0$. Figure 6(b) shows the evolution of the front position for $G = 1$ and $G = 0$. The final velocity, $dx_f/dt = 2Bh(x_f)$, is monotonically reached in both cases, but it decreases with time for $G = 0$, while the velocity increases for $G = 1$. Similarly to the case with $G = 0$, the velocity for $G = 1$ is independent of the molecular potential and the speed increases with A and B .

4. Intermediate contact angle: transition regime

4.1. Absence of gravity, $G = 0$

The transition regime appears for intermediate values of the contact angle θ . In contrast with previous section, here the effects of the molecular potential and the Marangoni stress are of the same order. We observe two different dynamics: a droplet

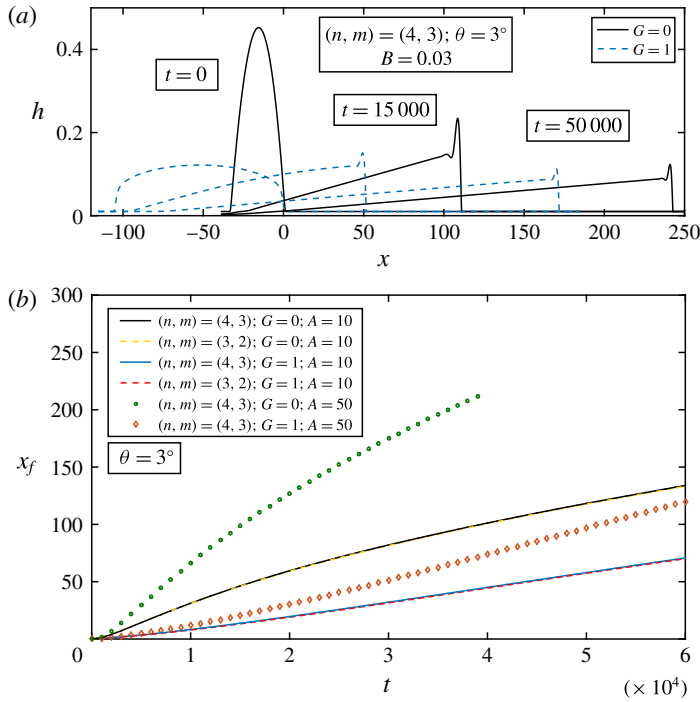


FIGURE 6. (Colour online) (a) Comparison of the thickness evolution with gravity $G = 1$ (dashed blue line) and without gravity $G = 0$ (black line). The position of the initial front is the same in both droplets. (b) Position of the front x_f versus time t for droplets with $\theta = 3^\circ$, $A = 10$, $h_* = 0.01$, $B = 0.01$ and several combination of (n, m) and G . For the dotted line, $A = 50$.

breaks into two or more smaller volumes, as reported Gomba & Homsy (2010), or it evolves to a steady profile that migrates with a constant velocity without breakups.

Figure 7 shows the evolution of the thickness profile for $(n, m) = (3, 2)$, $\theta = 15^\circ$ and $G = 0$. As described in Gomba & Homsy (2010), the fluid breaks up into smaller droplets and the behaviour is quite complex. Nevertheless, we observe that before breakup, the droplet adopts a transient stage consisting in a linear profile followed by a (short length) almost-flat thickness h_e (see $t = 4000$ in the figure). We will show that this thickness determines the later dynamics of the flow.

In figure 8, we keep all the parameters of the previous figure but we change the pair of the molecular potential to $(n, m) = (4, 3)$. Here, instead of the rupture observed for polar liquids, we observe that a steady profile is adopted after a transition stage. The initial shape evolves into a flat droplet with a capillary ridge at the front, which migrates with a constant velocity. This droplet shape has not been reported before.

Thus, in the transition regime a constant height h_e emerges, and the dynamics of the flow depends on the stability of that thickness. In the next two subsections, we analyse the parametric dependence of h_e and also the occurrence of breakups. Finally, we explore the effect of gravity.

4.1.1. Migration of flat droplets

We first analyse flat droplets, i.e. steady solutions that do not break up, move with a constant velocity and present a characteristic flat thickness h_e . Figure 9(a) shows the

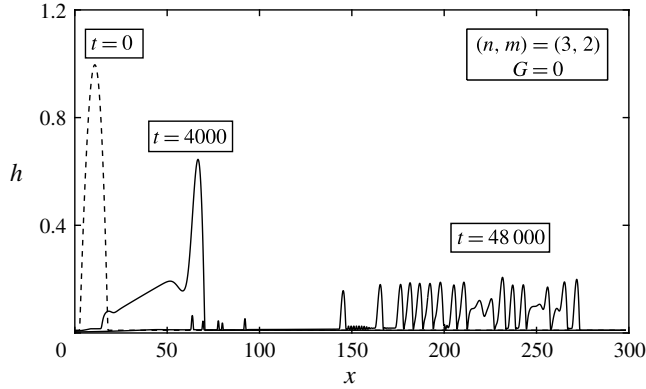


FIGURE 7. Evolution of the thickness profile with $\theta = 15^\circ$, $G = 0$, $h_* = 0.01$, $B = 0.03$ and $(n, m) = (3, 2)$. The droplet with initial cross-sectional area $A = 10$ breaks into smaller droplets.

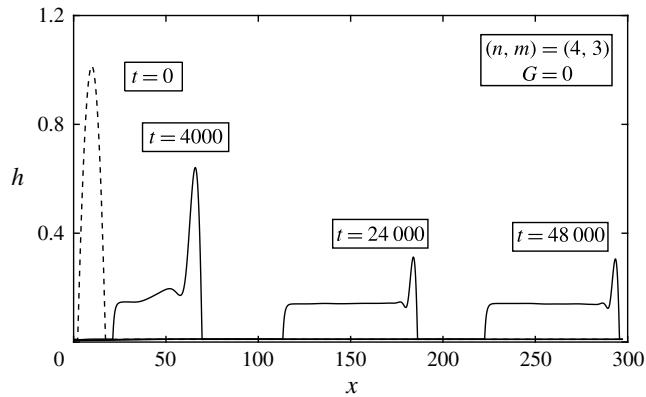


FIGURE 8. Evolution of the thickness profile with $\theta = 15^\circ$, $G = 0$, $h_* = 0.01$, $(n, m) = (4, 3)$, $B = 0.03$ and $A = 10$. The change of the molecular potential stabilizes the profile.

profiles for $\theta = 15^\circ$, $A = 10$ and several values of B at $t = 2.4 \times 10^4$, when the steady profile is completely developed. As B increases, the width of the profile w and the velocity of the droplet U increases, while the thickness h_e decreases. Note that the area below the capillary ridge enlarges as B diminishes and, when most of the fluid is within the capillary ridge, the profile does not present a flat film, such as in the case with $B = 0.01$. In figure 9(b) we set $\theta = 18^\circ$. If we compare these profiles with those with $\theta = 15^\circ$, we observe that for the same values of B , a larger θ implies a shorter w , and larger values for h_e and U .

Simulations show that w increases with A , while h_e is independent of A . Dimensional analysis and parametric studies on K , B and A allows us to determine how the different parameters are related. We find that the dependence of h_e on K and B is given by

$$h_e \propto KB^{-2/3} \propto \tan^2 \theta B^{-2/3}. \tag{4.1}$$

Figure 10(a) shows a good agreement between (4.1) and the numerical data for several combinations of the parameters. To understand how w depends on A , K and B , we

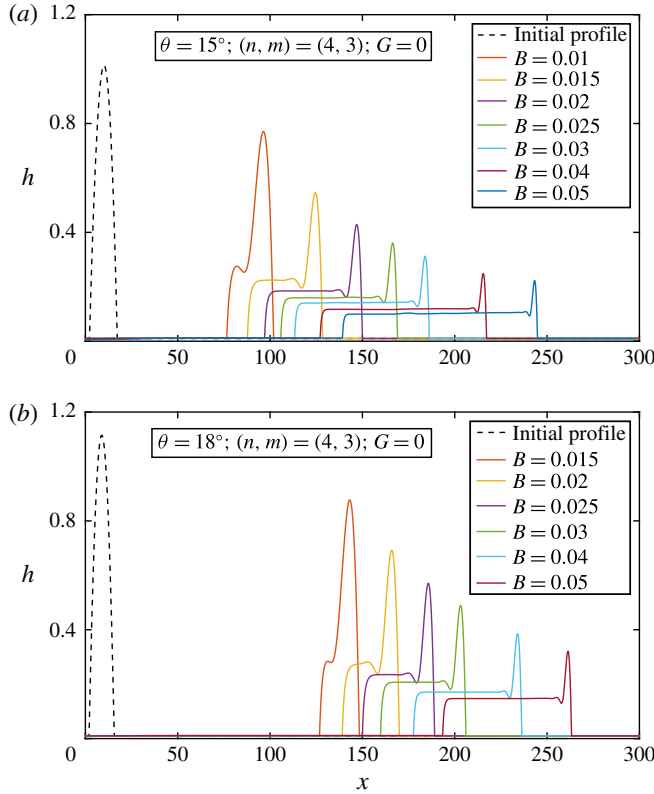


FIGURE 9. (Colour online) Profiles at $t = 2.4 \times 10^4$ in the evolution of a droplet with $A = 10$, $G = 0$, $h_* = 0.01$, $(n, m) = (4, 3)$ and initial contact angle (a) $\theta = 15^\circ$, and (b) $\theta = 18^\circ$. We observe that the thickness h_e , the width w and the velocity U depends on the thermal gradient B .

approximate the area A by:

$$A = \int h \, dx \sim h_e w, \tag{4.2}$$

and therefore the width follows the power law

$$w \propto \frac{A}{K} B^{2/3} \propto \frac{A}{\tan^2 \theta} B^{2/3}. \tag{4.3}$$

This expression is successfully tested in figure 10(b). Also, the numerical results show that when A is increased, the width w increases but the thickness h_e remains constant, as expected from (4.1) and (4.3).

As mentioned, the droplets finally move with a constant velocity U . To estimate U , we assume that the solution is well represented by a travelling wave of the form $h(x, t) \equiv h(\eta)$, with $\eta = x - Ut$. After integration, equation (2.10) becomes

$$h^3 \frac{d^3 h}{d\eta^3} + Kh^3 \frac{d}{d\eta} \left[\left(\frac{h_*}{h} \right)^n - \left(\frac{h_*}{h} \right)^m \right] - Gh^3 \frac{dh}{d\eta} + Bh^2 - Uh = \mathcal{V}, \tag{4.4}$$

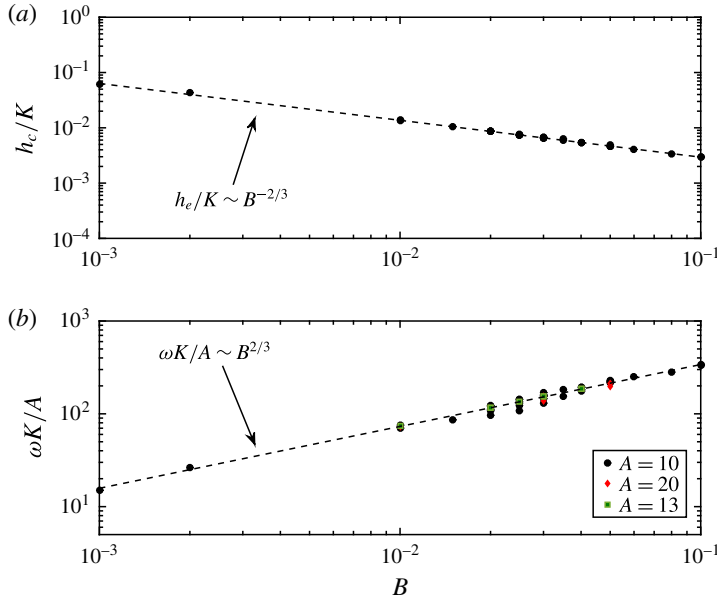


FIGURE 10. (Colour online) Dependence of (a) h_e and (b) w on the parameters of the problem B , θ and A . The dashed lines are the derived analytical expressions.

with \mathcal{V} a constant of integration. At the flat film, where $h = h_e$, the first and third derivatives are negligible, i.e.

$$\left. \frac{dh}{d\eta} \right|_{h=h_e} = \left. \frac{d^3h}{d\eta^3} \right|_{h=h_e} = 0, \tag{4.5}$$

and then,

$$U = Bh_e - \frac{\mathcal{V}}{h_e}. \tag{4.6}$$

Similarly, at $h = h_*$, the same conditions (4.5) apply, and (4.4) becomes

$$U = Bh_e \left(1 + \left(\frac{h_*}{h_e} \right) \right). \tag{4.7}$$

Assuming $h_*/h_e \ll 1$, the velocity of migration is $U = Bh_e$, which using (4.1) becomes

$$U \propto KB^{1/3} \propto \tan^2 \theta B^{1/3}. \tag{4.8}$$

Figure 11 confirms this dependence of U on the parameters K and B .

4.1.2. Occurrence of breakup

For intermediate contact angles, most of the cases with polar liquids break up into smaller droplets during the migration, while the rupture process with non-polar liquids was only observed for the highest values of B . Figure 12(a) shows the breakup of a droplet for $B = 0.05$ and $(n, m) = (4, 3)$. Although rupture is present, it only occurs

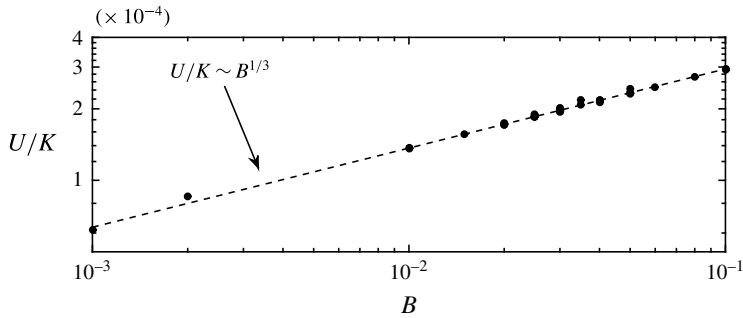


FIGURE 11. Dependence of the velocity U for several combination of the parameters B and K . The law (4.8) is valid for the intermediate flow regime when droplets moves steady without ruptures, as shown in figure 9.

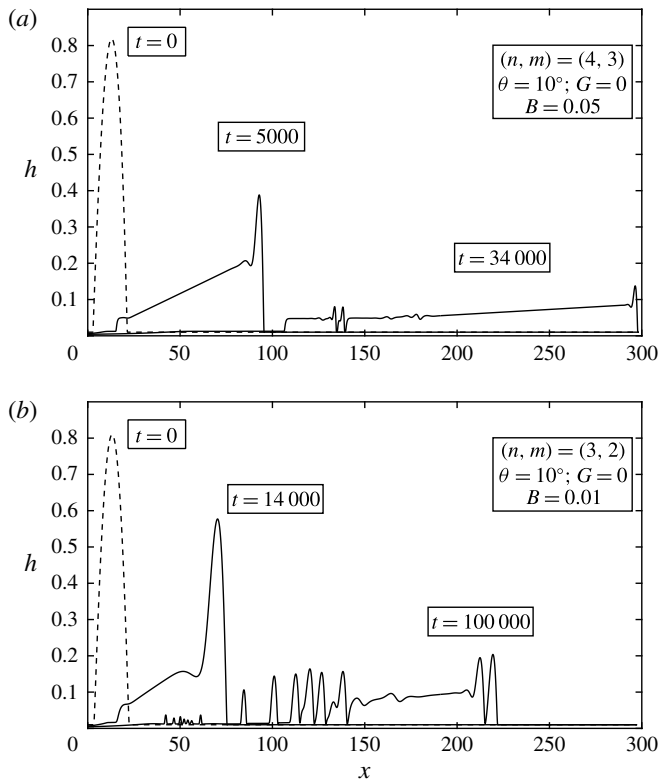


FIGURE 12. Evolution of the thickness profile with $\theta = 10^\circ$, $A = 10$, $h_* = 0.01$ and $G = 0$. (a) Non-polar liquid, $(n, m) = (4, 3)$ and thermal gradient $B = 0.05$. (b) Polar liquid, $(n, m) = (3, 2)$ and $B = 0.01$.

for late times and in few points when compared with the cases with $(n, m) = (3, 2)$. On the contrary, figure 12(b) shows a multiple droplet breakup occurring for $B = 0.01$ and $(n, m) = (3, 2)$. Therefore, simulations show that the molecular potentials and the Marangoni force clearly play a role in the stability of the flat film.

Case	λ_m^t theoretical	λ_m^n numerical
$\theta = 10^\circ; B = 0.01$	7.02	7.56
$\theta = 15^\circ; B = 0.03$	5.39	5.67
$\theta = 18^\circ; B = 0.05$	4.94	5.26

TABLE 2. Comparison of theoretical λ_m^t , equation (4.13) and numerical λ_m^n wavelengths.

The molecular potential, i.e. the nature of polar or non-polar liquid, manages the stability of the flat film. In order to understand the rupture process, we implement a linear stability analysis assuming that $h = h_e + \xi$, with $\xi \ll h_e$. After linearization, equation (2.10) becomes

$$\frac{\partial \xi}{\partial t} + \frac{\partial}{\partial x} \left[h_e^3 \left(\frac{\partial^3 \xi}{\partial x^3} + K' \frac{\partial \xi}{\partial x} \right) \right] + 2Bh_e \frac{\partial \xi}{\partial x} = 0, \quad (4.9)$$

with

$$K' = K \left(m \frac{h_*^m}{h_e^{m+1}} - n \frac{h_*^n}{h_e^{n+1}} \right). \quad (4.10)$$

We replace $\xi \sim \exp(ikx + \omega t)$ and obtain the following dispersion equation

$$\omega = -2iBh_e k - h_e^3 k^2 (k^2 - K'). \quad (4.11)$$

A stable constant thickness h_e has to satisfy $Re[\omega] < 0$, i.e.

$$k > \sqrt{K} \left(m \frac{h_*^m}{h_e^{m+1}} - n \frac{h_*^n}{h_e^{n+1}} \right)^{1/2}, \quad (4.12)$$

and the mode with the largest growth rate is

$$k_m = \sqrt{\frac{K}{2}} \left(m \frac{h_*^m}{h_e^{m+1}} - n \frac{h_*^n}{h_e^{n+1}} \right)^{1/2}. \quad (4.13)$$

Figure 13 shows the dispersion relationship for different values of θ and both molecular potentials. Comparing cases with the same value of B and A , the growth rate is always notably smaller for the pair $(n, m) = (4, 3)$ than for the $(n, m) = (3, 2)$. Also, the minimum unstable wavelength is larger for the case $(n, m) = (4, 3)$. Thus, non-polar liquids needs longer times and larger domains to develop an instability.

To estimate the distance between droplets, we implement a Fourier analysis of the thickness profile. Figure 14 shows the Fourier transform of the thickness profiles obtained for $(n, m) = (3, 2)$ and different values of B . The position of the vertical line, that indicates the maximum wavelength amplitude λ_m^n , agrees well with the theoretical value $\lambda_m^t = 2\pi/k_m$ as shown in table 2. Thus, the number of droplets and the distance between them can be predicted from a linear stability analysis.

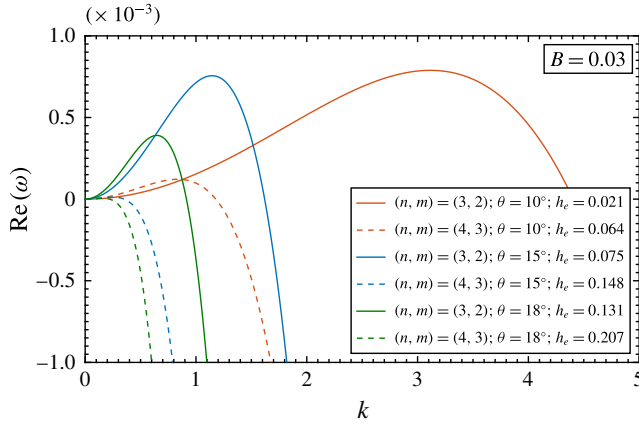


FIGURE 13. (Colour online) Relation of dispersion (4.11) for different combination of the parameters. The thickness h_e is estimated in the transition stage. Same colour is used for cases with same θ and A .

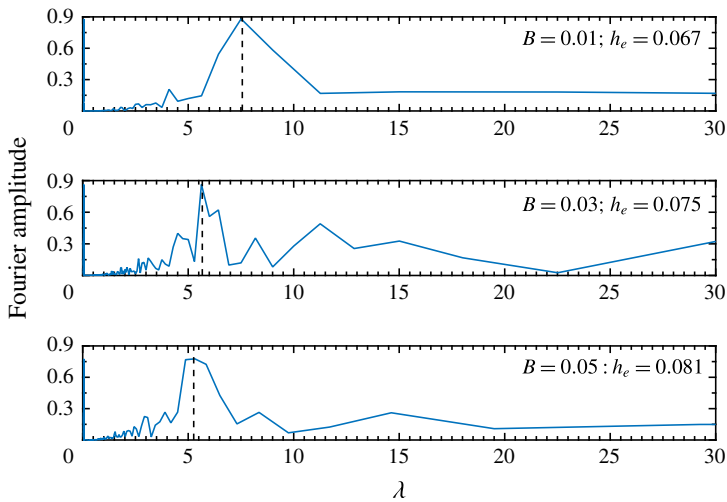


FIGURE 14. (Colour online) Fourier transform of the thickness profile with a molecular potential $(n, m) = (3, 2)$ and three different values of B . The vertical line points the maximum wavelength λ_m^n .

4.2. Effect of gravity, $G = 1$

Figure 15 shows the evolution of the thickness profile for $\theta = 15^\circ$, $B = 0.01$, $G = 1$ and both molecular potentials. Gravity compresses the profiles in the z direction, softens the valley that appears immediately behind the capillary ridge and increases the width of the initial profile (compare with the profiles in figures 7 and 9). More interesting, under the action of gravity the breakups are not observed.

We study how gravity affects the stability of flat profiles. A linear stability analysis shows that the growth rate is now given by

$$\omega = -2iBh_e k - h_e^3 k^2 (k^2 - (K' - G)), \tag{4.14}$$

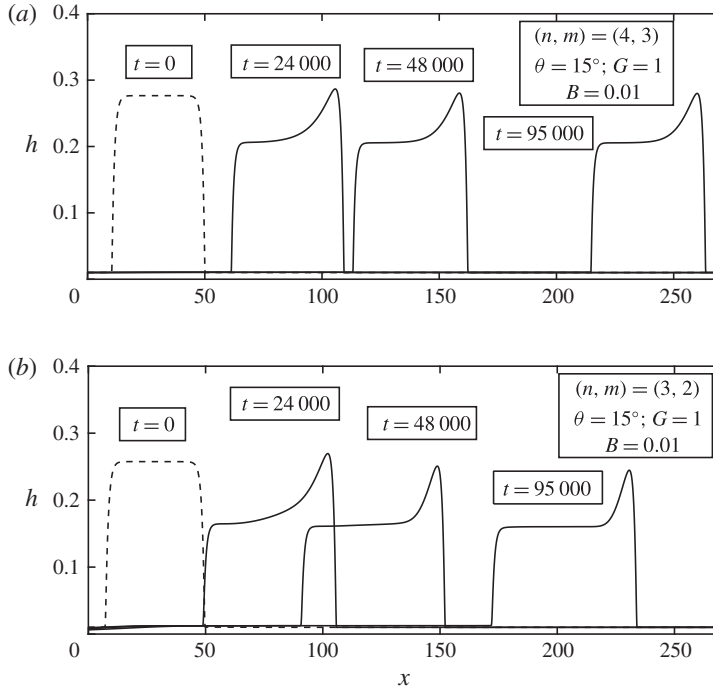


FIGURE 15. Evolution of the thickness profile for a droplet with $\theta = 15^\circ$, $A = 10$, $G = 1$, $h_* = 0.01$ and $B = 0.01$. (a) Non-polar liquid, $(n, m) = (4, 3)$. (b) Polar liquid, $(n, m) = (3, 2)$.

and then, a uniform film h_e is stable if the wavenumber satisfies

$$k > (K' - G)^{1/2}. \tag{4.15}$$

Figure 16 shows that the effect of G is to decrease the real part of the growth rate ω and the mode k_m . Thus, situations where breakup is observed with $G = 0$ may not present ruptures with $G = 1$, as in the cases for $B = 0.03$ and $(n, m) = (3, 2)$ shown in figures 7 and 17. Nevertheless, figure 17 shows that breakup for $G = 1$ and polar liquids may occur for larger values of B . Breakup of a polar liquid in the presence of gravity can be understood in the following way: assuming that the relation $h_e \propto B^{-\beta}$ (with $\beta > 0$) is still valid when $G = 1$ (later this is confirmed), if the thermal gradient B increases, the thickness of the stable film h_e decreases. Then, from (4.10) K' increases and finally, from (4.15), the smallest wavenumber of a stable mode becomes larger. Briefly, an increase of B is destabilizing. Added to this, when B is increased, the region with $h = h_e$ widens (w enlarges) and it is easier to fit unstable modes inside the drop.

Gravity also changes the dependence of h_e on the parameters. Figure 18(a) shows h_e/K against B for $G = 1$ for the two explored potentials (we also include cases with $G = 0$ to illustrate the difference in the exponent of the power law). For $G = 1$, the simulations show that the dependence of h_e on K and B is

$$h_e \propto K B^{-3/5} \propto \tan^2 \theta B^{-3/5}. \tag{4.16}$$

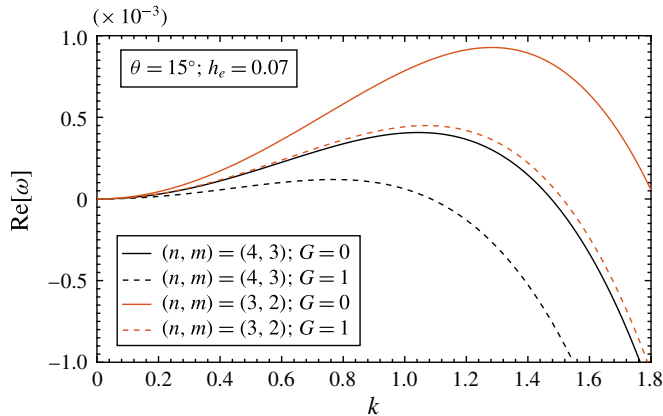


FIGURE 16. (Colour online) Effect of gravity on the growth rate. Here, $\theta = 15^\circ$ and $h_e = 0.07$. The maximum of ω and the largest unstable k decrease when $G = 1$ compared with the case $G = 0$.

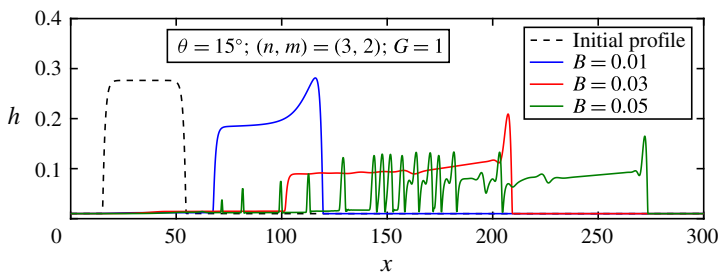


FIGURE 17. (Colour online) Profiles at $t = 2.7 \times 10^4$ in the evolution of a droplet with initial contact angle $\theta = 15^\circ$, $A = 10$, $G = 1$, $h_* = 0.01$ and $(n, m) = (3, 2)$. In contrast with the observed evolution for the case with $G = 0$, here the case with $B = 0.01$ does not present a breakup when gravity is considered.

Since for a given value of θ , K is higher for non-polar than for polar liquids, the value of h_e is higher for the pair $(n, m) = (4, 3)$. Then, equation (4.7) predicts that the velocity of migration is higher for non-polar liquids than for polar liquids. Effectively, figure 18(b) shows that both h_e and U are larger for the pair $(n, m) = (4, 3)$.

5. Large contact angles: droplet regime

5.1. Absence of gravity, $G = 0$

For large contact angles, the value of K increases and the molecular potential becomes strong enough to keep the initial shape of the droplet during the migration. In the droplet regime, the Marangoni stress displaces the droplet with constant velocity U without stretching it. Brzoska *et al.* (1993) and Chen *et al.* (2005) show experimentally that droplets migrate keeping their initial shape. In their experiments, the velocity increases with the footprint R of the wet surface, but different liquids present differences in the dependence of U on R . This leads us to think that the type of the molecular force should modify the velocity of migration. Figure 19 shows the evolution of the thickness profile for a droplet with area $A = 10$, initial contact angle

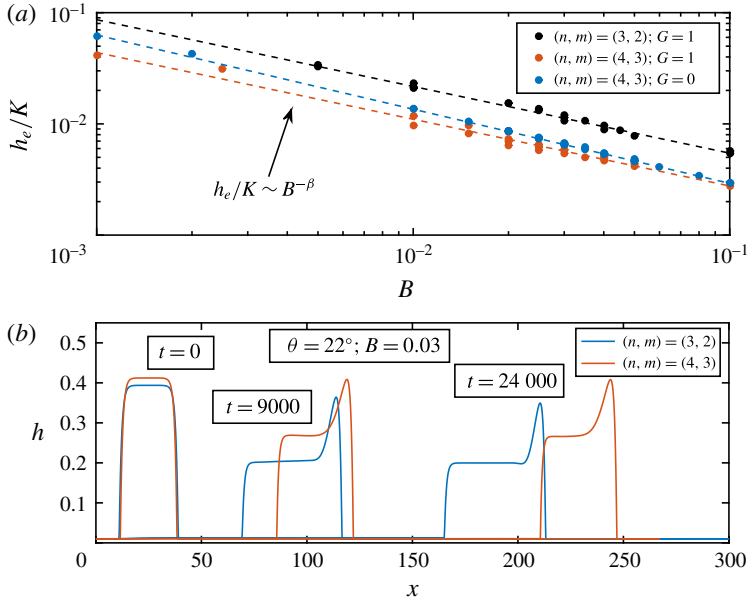


FIGURE 18. (Colour online) (a) Dependence of the thickness h_e for several combinations of B and θ . (b) Evolution of the thickness profile with $\theta = 22^\circ$, $A = 10$, $G = 1$, $h_* = 0.01$, $B = 0.03$ and both molecular potentials.

$\theta = 25^\circ$ and thermal gradient $B = 0.01$, for both molecular potentials. Effectively, the velocity of migration changes with the polarity of the liquid.

In this regime, front and rear contact lines move with the same constant velocity U . Brzoska *et al.* (1993) and Chen *et al.* (2005) have shown that the velocity is proportional to B and inversely proportional to the viscosity. Gomba & Homsy (2010) demonstrated, by means of dimensional analysis, that the velocity for droplets with $(n, m) = (3, 2)$ supports this experimental conclusion. The latter authors constructed two Π^* groups and, using numerical results, explored the relationship between them. They found that the velocity is given by

$$\Pi_1^* = \frac{U}{Bh_*} \propto (\Pi_2^*)^\beta, \tag{5.1}$$

with $\beta = 0.4$ for the case $(n, m) = (3, 2)$ and $G = 0$. Here, we generalize the previous result considering that the pair (n, m) could change depending on the type of liquid. Then, we define the dimensionless number

$$\Pi_2^* = \left(\frac{(n-1)(m-1)}{2(n-m)} \right)^{1/2} \frac{A \tan \theta}{h_*^2}. \tag{5.2}$$

Figure 20 shows U/Bh_* versus $A \tan \theta/h_*^2$ for several combinations of the parameters (n, m) , A , θ , B and h_* . Interestingly, the exponent in (5.1) is $\beta = 0.40$, independently of the pair (n, m) . Therefore, the pre-factor in (5.2) is responsible of the different velocity for each liquid.

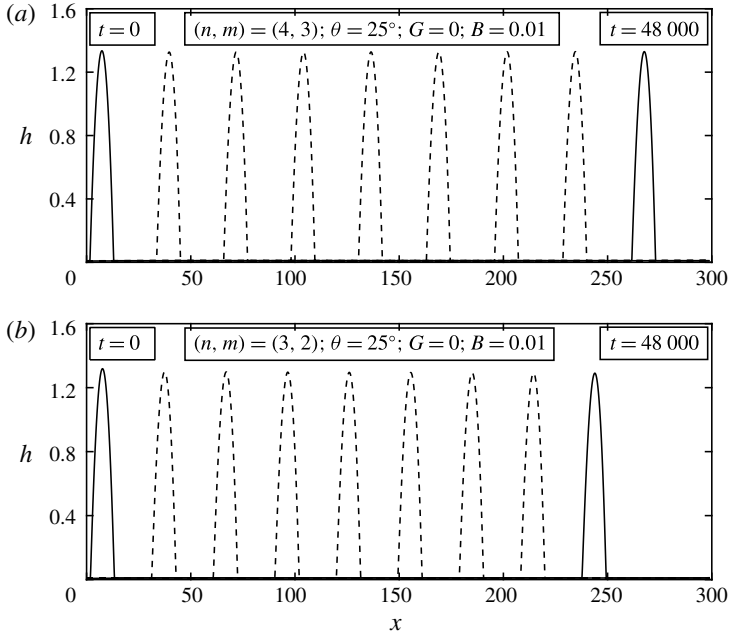


FIGURE 19. Evolution of the thickness profile for (a) non-polar liquid, $(n, m) = (4, 3)$ and (b) polar liquid, $(n, m) = (3, 2)$, until $t = 4.8 \times 10^4$. The effect of the potential avoids drop stretching due to Marangoni stress. Here, $\Delta t = 6 \times 10^3$, $\theta = 25^\circ$, $A = 10$, $G = 0$, $h_* = 0.01$ and $B = 0.01$.

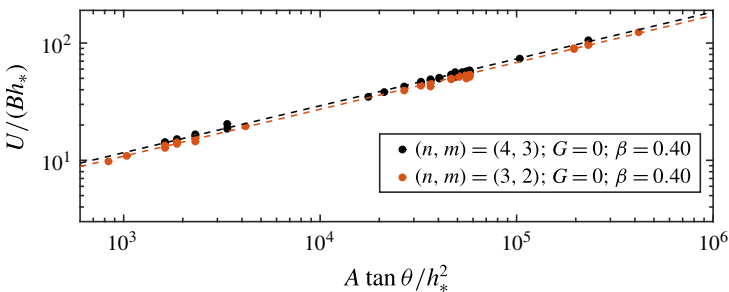


FIGURE 20. (Colour online) Dependence of the velocity U for several combination of the parameters (n, m) , A , θ , B and h_* .

5.2. Effect of gravity, $G = 1$

Gravity produces similar results to those observed in previous regimes. Figure 21 shows the evolution of a droplet with $A = 10$, $\theta = 25^\circ$, $B = 0.01$ and $G = 1$, for both molecular potentials. Here, the initial profile is wider and has a lower height than the corresponding case with $G = 0$. When the thermal gradient is applied, the droplet slightly modified its shape. After a short time, the droplet migrates with a steady profile, but its velocity is smaller than the case with $G = 0$, as shown in figures 19 and 21.

Figure 22 shows U/Bh_* versus $A \tan \theta / h_*^2$ for several combination of the parameters (n, m) , A , θ , B , h_* and G . Gravity has a noticeable effect on the power law exponent.

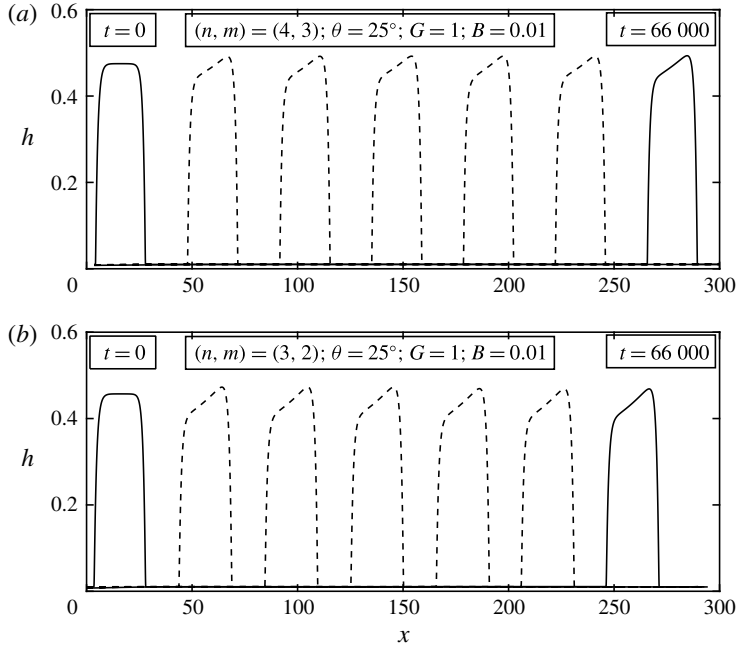


FIGURE 21. Evolution of the thickness profile for (a) $(n, m) = (4, 3)$ and (b) $(n, m) = (3, 2)$, until $t = 6.6 \times 10^4$. Here, $\Delta t = 1.1 \times 10^4$, $\theta = 25^\circ$, $A = 10$, $G = 1$, $h_* = 0.01$ and $B = 0.01$.

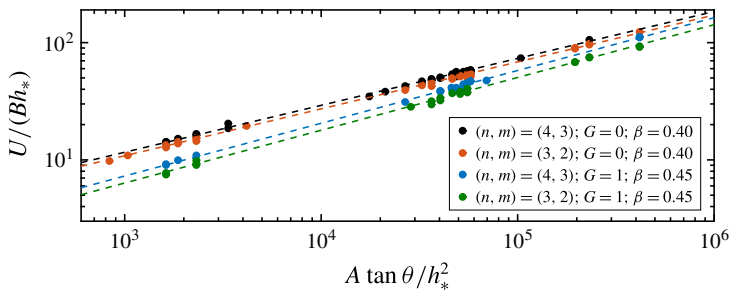


FIGURE 22. (Colour online) Dependence of the velocity U for several combinations of the parameters (n, m) , A , θ , B , h_* and G .

Effectively, for $G = 1$ ($G = 0$), the exponent is $\beta = 0.45$ ($\beta = 0.40$), with β independent of n and m . Due to the fact that the exponents are different in each case, the results suggest that the droplet could migrate with a larger velocity for $G = 1$ than for $G = 0$. In addition, we can see from the figure that for a given value of G , polar liquids migrate always with a velocity U smaller than non-polar ones.

6. Discussions and conclusions

In this paper, the fate of droplets subject to a thermocapillary driving force is investigated numerically with a particular emphasis on the effects of the form of the molecular interaction potential and gravity. The droplet dynamics model is based on

the lubrication approximation and the resulting partial differential equation is solved in the finite element package COMSOL. The study confirms earlier observations that three regimes exist depending on the value of the contact angle.

For small contact angles, the film regime is observed for which the droplet stretches with the advancing contact line moving substantially faster than the receding one, leading to an increasing droplet footprint and a decreasing maximum thickness. The balance between viscous and Marangoni stresses produces a linear profile behind the capillary ridge at the front, analogous to the self-similar solution observed for falling films on solid substrates (Huppert 1982; Gomba *et al.* 2005, 2007). This regime is well described by the similarity solution given by Gomba & Homsy (2010) irrespective of the molecular interaction potential which is a consequence of the fact that for small contact angles, the contribution of the disjoining pressure term is negligible. The effect of gravity is to delay the development of this similarity solution which is still reached for larger times but with a decreased height of the capillary ridge at the advancing contact line. The asymptotic velocity of the front is given by $U = \sqrt{BA/t}$.

For intermediate values of the contact angle, the transition regime occurs. In this regime, the droplet either travels with a constant profile which is different from the initial one or breaks up into a series of smaller droplets. In the former case, the droplet is found to travel with a constant velocity which scales as the 1/3 power of the thermocapillary driving stress and is proportional to K , i.e. small differences in the contact angle produce noticeable effects on the velocity, as shown in figure 9. In the latter case, the outcome is found to be strongly dependent of the molecular interaction potential. For polar liquids with a disjoining pressure given by the pair $(n, m) = (3, 2)$, breakup occurs more readily than for non-polar liquids with a disjoining pressure for which $(n, m) = (4, 3)$. In other words, it takes a smaller value of the driving thermocapillary stress to break up the initial droplets into smaller ones for polar liquids than for non-polar ones. This feature is explained by a linear stability analysis of the uniform film which develops as the droplet evolves in the intermediate regime. This linear stability analysis reveals that the maximum growth rate of the instability is larger for polar liquids, $(n, m) = (3, 2)$ than for non-polar ones and occurs for shorter wavelengths. In other words, the instability for non-polar liquids takes longer times and larger distances to develop. The stability analysis also allows a prediction of the number of droplets the parent droplet breaks up into and the distance between them. The effect of gravity on the growth of the instability is to decrease the maximum growth rate and shift it to larger wavelengths.

For larger values of the contact angle, the model confirms earlier observations that the droplet travels with a constant profile and at constant speed towards the colder part of the substrate. The travelling velocity is found to be greater for non-polar than for polar liquids and scales linearly with the thermocapillary driving force with or without gravity. Interestingly, the exponent of the law is found to be independent of model of the disjoining pressure term, i.e. independent of n and m , but it depends on the gravity. We expect that for a different combination of parameters, the travelling velocity will be greater for the case with gravity. The effect of gravity in that case is to modify slightly the droplet profile as it travels on the substrate. Table 3 summarizes the description of the velocities of droplets for each regime, for polar and non-polar liquids and considering or not the effect of gravity.

The results allow us to discuss the points raised in § 1 about experimental observations. These are: (i) the saturation in the curve U versus R , (ii) the elongation of large droplets and (iii) the non-occurrence of breakups.

Regime	Molecular potential (n, m)	Gravity G	Velocity U
Film	(4, 3); (3, 2)	0; 1	$\sqrt{BA/t}$
Transition	(4, 3)	0	$KB^{1/3}$
(no ruptures)	(4, 3); (3, 2)	1	$KB^{2/5}$
Droplet	(4, 3); (3, 2)	0	$Bh_*(A\sqrt{K/h_*^3})^{0.40}$
	(4, 3); (3, 2)	1	$Bh_*(A\sqrt{K/h_*^3})^{0.45}$

TABLE 3. Velocity of droplets for each regime depending on the molecular and gravitational effects. The velocities for the transition regime are for cases without breakups.

Brzoska *et al.* (1993) show in their figure 2 the velocity of the droplets versus the footprint, R . While for the smallest droplets in the experiments ($1 < R < 4$), the velocity follows a roughly linear dependence on R , from $R \geq 4$ the experimental curve suggests that the velocity starts to converge to a saturation value. The authors attribute the change in the curve to the effect of gravity, despite the fact that gravity is expected to have an effect from smaller values of R , i.e. for $R \geq 1$.

Our results show that gravity is not needed to explain the change in the behaviour of U , and that gravity effectively has an effect from $R = 1$. Under non-gravity conditions, it is observed that as A is increased, the velocity first follows a dependence with $A^{0.4}$ in the droplet regime, to later saturate to a velocity $U \propto KB^{1/3}$ when flat droplets emerge due to the presence of the Marangoni stress (§4.1.1). When gravity is included to match experimental conditions, droplets with $R < 1$ also displace with a velocity $U \propto A^{0.4}$ because the effect of gravity is negligible. Middle size droplets ($1 < R < 4$) move with $U \propto A^{0.45}$, and larger droplets migrate with a velocity $U \propto KB^{2/5}$.

Figure 23 shows U versus R (both dimensionless), in the same fashion as in the experimental works. Let us first focus on the curve for $G = 1$. Notice that for $R < 1$ we have $U \propto R^{0.72}$. For $1 < R < 4$, $U \propto R^{0.45}$ which is easily explained because as gravity is not negligible, $A \propto R$. Finally, for $R > 4$ the velocity saturates. The inset of figure 23 shows the same data in a regular plot: the points with $1 < R < 4$ resembles the ‘almost linear’ dependence observed in the experiments for $R < 4$. The saturation of U for $R \approx 4$ is observed for both $G = 1$ and $G = 0$, as occurs in experiments. Therefore, the saturation of U is due to the change of the dynamics from droplet to transition regimes, and not to the action of gravity.

Brzoska *et al.* (1993) also tracked the shape of the perimeter of the moving droplet, and observed that smaller ones almost keep their initial shape, while larger ones elongate in the direction of displacement. In figure 6 of their work, the authors present the ratio of the elongation on the initial radius against the initial radius: the relative elongation is stronger for larger volume droplets. Our simulations show, effectively, that the relative elongation is larger for $R > 4$ without the need for the action of gravity. Again, the change is due to the transition from ‘droplet’ to ‘transition’ regime.

Another important issue connected with the elongation of the droplet is the non-occurrence of the breakup in experiments, as predicted by Gomba & Homsy (2010). Here, we show that, when a non-polar liquid is considered, the droplet elongates but does not break up into smaller droplets, as shown in §4. The instability of the bulk region behind the bump is found to be sensitive both to the effects of

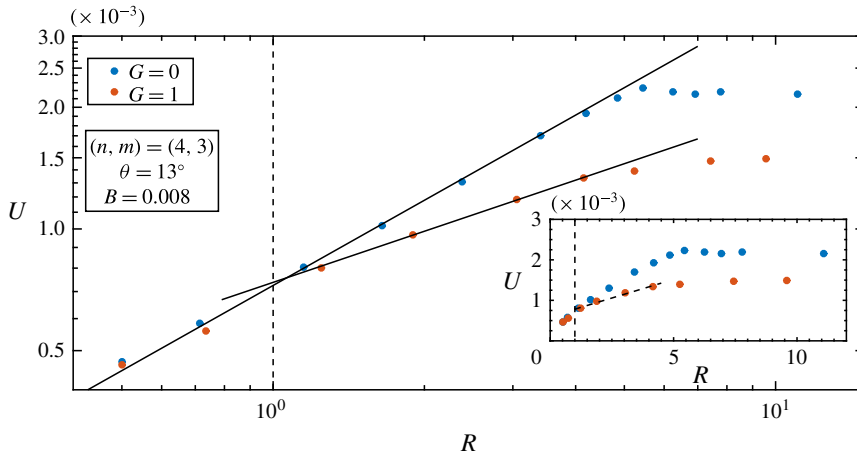


FIGURE 23. (Colour online) Log–log plot of the velocity against the footprint of the droplets (both are dimensionless, $B = 0.008$, $\theta = 13^\circ$). The plot clearly shows three different behaviours for U when $G = 1$. For $R < 1$, gravity is negligible and $U \propto R^{0.72}$. For $1 < R < 4$, $U \propto R^{0.45}$ due to the action of gravity. Larger droplets present a saturation with a velocity $U = Bh_e$ when the dynamics switches from ‘droplet’ to ‘transition’ regime. For $G = 0$, U also presents a saturation at $R \approx 4$, as in the experiments. The inset shows the same data, in regular coordinates, as in figure 2 of Brzoska *et al.* (1993).

gravity and the polarity of the liquid. As shown in figure 16, polar liquids present a larger growth rate than non-polar ones. Furthermore, as the shorter unstable mode of a polar liquid is smaller than the corresponding one for non-polar liquids, the instability of the latter requires larger domains than the former to develop, i.e. more stretched droplets. Gravity has a similar effect, reducing both the growth rate (the maximum growth rate $\omega_{max} = h_e^3(K' - G)^2/4$), and the shorter unstable mode, $k_c = (K' - G)^{1/2}$. In conclusion, the polar nature of the liquid is an important parameter to consider to correctly account for the experimental results. Experimentalists should employ polar liquids or stronger thermal gradients in order to observe, under gravity conditions, the breakup of drops.

Summarizing, this study provides new insights on the fate of partially wetting droplets subject to a non-uniform, linearly varying temperature field. It also provides new guidelines on how to select fluid properties and operating conditions to achieve a desired wetting outcome which may be of importance, for example, in the context of droplet actuation in open microfluidics devices.

Acknowledgements

The authors gratefully acknowledge the funding supports via the CONICET grants PIP no. 356 and PIP no. 299, the ANPCyP grant no. 2012-1707 and CICIPBA.

REFERENCES

- BROCHARD-WYART, F. 1989 Motion of droplets on solid surfaces induced by chemical or thermal gradients. *Langmuir* **5** (3), 432–438.
- BRZOSKA, J. B., BROCHARD-WYART, F. & RONDELEZ, F. 1993 Motions of droplets on hydrophobic model surfaces induced by thermal gradients. *Langmuir* **9** (8), 2220–2224.

- CACHILE, M., SCHNEEMILCH, M., HAMRAOUI, A. & CAZABAT, A. M. 2002 Films driven by surface tension gradients. *Adv. Colloid Interface Sci.* **96** (1), 59–74.
- CAMPANA, D. M., UBAL, S., GIAVEDONI, M. D., SAITA, F. A. & CARVALHO, M. S. 2016 Three dimensional flow of liquid transfer between a cavity and a moving roll. *Chem. Engng Sci.* **149**, 169–180.
- CASADEVALL I SOLVAS, X. & DEMELLO, A. 2011 Droplet microfluidics: recent developments and future applications. *Chem. Commun.* **47** (7), 1936–1942.
- CHAUDHURY, K. & CHAKRABORTY, S. 2015 Spreading of a droplet over a nonisothermal substrate: multiple scaling regimes. *Langmuir* **31** (14), 4169–4175.
- CHEN, J. Z., TROIAN, S. M., DARHUBER, A. A. & WAGNER, S. 2005 Effect of contact angle hysteresis on thermocapillary droplet actuation. *J. Appl. Phys.* **97** (1), 014906.
- CHOI, K., NG, A. H. C., FOBEL, R. & WHEELER, A. R. 2012 Digital microfluidics. *Annu. Rev. Anal. Chem.* **5** (1), 413–440.
- CRASTER, R. V. & MATAR, O. K. 2009 Dynamics and stability of thin liquid films. *Rev. Mod. Phys.* **81** (3), 1131–1198.
- DAI, Q., KHONSARI, M. M., SHEN, C., HUANG, W. & WANG, X. 2017 On the migration of a droplet on an incline. *J. Colloid Interface Sci.* **494**, 8–14.
- DERJAGUIN, B. V. & CHURAEV, N. V. 1974 Structural component of disjoining pressure. *J. Colloid Interface Sci.* **49** (2), 249–255.
- DERJAGUIN, B. V., RABINOVICH, Y. I. & CHURAEV, N. V. 1978 Direct measurement of molecular forces. *Nature* **272** (5651), 313–318.
- EHRHARD, P. & DAVIS, S. H. 1991 Non-isothermal spreading of liquid drops on horizontal plates. *J. Fluid Mech.* **229**, 365–388.
- EÖTVÖS, R. 1886 Ueber den Zusammenhang der Oberflächenspannung der Flüssigkeiten mit ihrem Molecularvolumen. *Annalen der Physik* **263** (3), 448–459.
- FORD, M. L. & NADIM, A. 1994 Thermocapillary migration of an attached drop on a solid surface. *Phys. Fluids* **6** (9), 3183–3185.
- FOTE, A. A., SLADE, R. A. & FEUERSTEIN, S. 1977 Thermally induced migration of hydrocarbon oil. *Trans. ASME J. Lubr. Technol.* **99** (2), 158–162.
- GASKELL, P. H., JIMACK, P. K., SELLIER, M. & THOMPSON, H. M. 2004 Efficient and accurate time adaptive multigrid simulations of droplet spreading. *Intl J. Numer. Meth. Fluids* **45** (11), 1161–1186.
- GLASNER, K. B. & WITELSKI, T. P. 2003 Coarsening dynamics of dewetting films. *Phys. Rev. E* **67** (1), 016302.
- GOMBA, J. M., DIEZ, J. A., GONZÁLEZ, A. G. & GRATTON, R. 2005 Spreading of a micrometric fluid strip down a plane under controlled initial conditions. *Phys. Rev. E* **71** (1), 016304.
- GOMBA, J. M., DIEZ, J. A., GRATTON, R., GONZÁLEZ, A. G. & KONDIC, L. 2007 Stability study of a constant-volume thin film flow. *Phys. Rev. E* **76** (4), 046308.
- GOMBA, J. M. & HOMSY, G. M. 2009 Analytical solutions for partially wetting two-dimensional droplets. *Langmuir* **25** (10), 5684–5691.
- GOMBA, J. M. & HOMSY, G. M. 2010 Regimes of thermocapillary migration of droplets under partial wetting conditions. *J. Fluid Mech.* **647**, 125–142.
- GOODWIN, R. & HOMSY, G. M. 1991 Viscous flow down a slope in the vicinity of a contact line. *Phys. Fluids A* **3** (1991), 515–528.
- GOTKIS, Y., IVANOV, I., MURISIC, N. & KONDIC, L. 2006 Dynamic structure formation at the fronts of volatile liquid drops. *Phys. Rev. Lett.* **97** (18), 186101.
- GUGGENHEIM, E. A. 1945 The principle of corresponding states. *J. Chem. Phys.* **13** (7), 253–261.
- HUEBNER, A., SHARMA, S., SRISA-ART, M., HOLLFELDER, F., EDEL, J. B. & DEMELLO, A. J. 2008 Microdroplets: a sea of applications? *Lab on a Chip* **8** (8), 1244–1254.
- HUPPERT, H. E. 1982 The propagation of two-dimensional and axisymmetric viscous gravity currents over a rigid horizontal surface. *J. Fluid Mech.* **121**, 43–58.
- KARAPETSAS, G., SAHU, K. C. & MATAR, O. K. 2013 Effect of contact line dynamics on the thermocapillary motion of a droplet on an inclined plate. *Langmuir* **29** (28), 8892–8906.

- KARAPETSAS, G., SAHU, K. C., SEFIANE, K. & MATAR, O. K. 2014 Thermocapillary-driven motion of a sessile drop: effect of non-monotonic dependence of surface tension on temperature. *Langmuir* **30** (15), 4310–4321.
- KARBALAEI, A., KUMAR, R. & CHO, H. 2016 Thermocapillarity in microfluidics – a review. *Micromachines* **7** (1), 13.
- MAC INTYRE, J. R., GOMBA, J. M. & PERAZZO, C. A. 2016 New analytical solutions for static two-dimensional droplets under the effects of long- and short-range molecular forces. *J. Engng Math.* **101** (1), 55–69.
- NGUYEN, H. B. & CHEN, J. C. 2010 A numerical study of thermocapillary migration of a small liquid droplet on a horizontal solid surface. *Phys. Fluids* **22** (6), 062102.
- ORON, A. & BANKOFF, S. G. 2001 Dynamics of a condensing liquid film under conjoining/disjoining pressures. *Phys. Fluids* **13** (5), 1107–1117.
- ORON, A., DAVIS, S. H. & BANKOFF, S. G. 1997 Long-scale evolution of thin liquid films. *Rev. Mod. Phys.* **69** (3), 931–980.
- PERAZZO, C. A. & GRATTON, J. 2004 Navier–Stokes solutions for parallel flow in rivulets on an inclined plane. *J. Fluid Mech.* **507**, 367–379.
- PERAZZO, C. A., MAC INTYRE, J. R. & GOMBA, J. M. 2014 Final state of a perturbed liquid film inside a container under the effect of solid–liquid molecular forces and gravity. *Phys. Rev. E* **89** (4), 043010.
- PRATAP, V., MOUMEN, N. & SUBRAMANIAN, R. S. 2008 Thermocapillary motion of a liquid drop on a horizontal solid surface. *Langmuir* **24** (7), 5185–5193.
- SCHWARTZ, L. W. & ELEY, R. R. 1998 Simulation of droplet motion on low-energy and heterogeneous surfaces. *J. Colloid Interface Sci.* **202** (1), 173–188.
- SCHWARTZ, L. W. & ROY, R. V. 2004 Theoretical and numerical results for spin coating of viscous liquids. *Phys. Fluids* **16** (3), 569–584.
- SMITH, M. K. 1995 Thermocapillary migration of a two-dimensional liquid droplet on a solid surface. *J. Fluid Mech.* **294**, 209–230.
- SOLOMENTSEV, Y. & WHITE, L. R. 1999 Microscopic drop profiles and the origins of line tension. *J. Colloid Interface Sci.* **218**, 122–136.
- STAROV, V. M., VELARDE, M. G. & RADKE, C. J. 2007 *Wetting and Spreading Dynamics*, Surfactant Science Series, p. 11. CRC Press.
- STONE, H. A., STROOCK, A. D. & AJDARI, A. 2004 Engineering flows in small devices. *Annu. Rev. Fluid Mech.* **36** (1), 381–411.
- SUR, J., BERTOZZI, A. L. & BEHRINGER, R. P. 2003 Reverse undercompressive shock structures in driven thin film flow. *Phys. Rev. Lett.* **90** (12), 126105.
- UBAL, S., CAMPANA, D. M., GIAVEDONI, M. D. & SAITA, F. A. 2008 Stability of the steady-state displacement of a liquid plug driven by a constant pressure difference along a prewetted capillary tube. *Ind. Engng Chem. Res.* **47** (16), 6307–6315.